IOP Publishing
Superconductor Science and Technology
Supercond. Sci. Technol. 31 (2018) 045008 (15pp)
https://doi.org/10.1088/1361-6668/aaafaa

Stress analysis in high-temperature superconductors under pulsed field magnetization

Haowei Wu, Huadong Yong[1] and Youhe Zhou[1]

Key Laboratory of Mechanics on Disaster and Environment in Western China, Ministry of Education of China, and Department of Mechanics and Engineering Sciences, College of Civil Engineering and Mechanics, Lanzhou University, Lanzhou, Gansu 730000, People's Republic of China

E-mail: yonghd@lzu.edu.cn and zhouyh@lzu.edu.cn

Received 17 December 2017, revised 23 January 2018
Accepted for publication 15 February 2018
Published 8 March 2018

Abstract

Bulk high-temperature superconductors (HTSs) have a high critical current density and can trap a large magnetic field. When bulk superconductors are magnetized by the pulsed field magnetization (PFM) technique, they are also subjected to a large electromagnetic stress, and the resulting thermal stress may cause cracking of the superconductor due to the brittle nature of the sample. In this paper, based on the H-formulation and the law of heat transfer, we can obtain the distributions of electromagnetic field and temperature, which are in qualitative agreement with experiment. After that, based on the dynamic equilibrium equations, the mechanical response of the bulk superconductor is determined. During the PFM process, the change in temperature has a dramatic effect on the radial and hoop stresses, and the maximum radial and hoop stress are 24.2 MPa and 22.6 MPa, respectively. The mechanical responses of a superconductor for different cases are also studied, such as the peak value of the applied field and the size of bulk superconductors. Finally, the stresses are also presented for different magnetization methods.

Keywords: high-temperature superconductor, pulsed field magnetization, electromagnetic stress, thermal stress, mechanical response

(Some figures may appear in colour only in the online journal)

1. Introduction

Superconducting materials have received much attention because of their unique electromagnetic properties. Their high critical current density and their ability to trap a large field enable high-temperature superconductors (HTSs) to be widely used in energy storage flywheels, magnetic levitation, magnetic separation, magnetic resonance imaging and rotating machines [1–7]. The traditional methods used to magnetize a bulk superconductor are the field-cooling (FC) magnetization and zero-field-cooling (ZFC) magnetization techniques [8]. ZFC refers to the situation where the superconductors are cooled without an applied magnetic field, and then an external magnetic field is applied. Conversely, FC refers to the situation where the external magnetic field is applied first, and then the superconductors are cooled [9]. Based on the FC method, a high trapped magnetic field of 17.6 T was obtained [10], which is the largest field up to now. However, FC magnetization requires a large magnetizing fixture, which is not convenient for practical application [9]. Recently, the pulsed field magnetization (PFM) technique has been considered as a substitute for the traditional methods. The advantages of PFM are that it is compact, mobile and relatively inexpensive [11, 12]. For PFM, the magnetic field is applied for a few milliseconds, which will result in a large temperature rise so that the trapped field is reduced [13]. The field trapped by PFM is usually lower than in traditional magnetization methods, and the largest field trapped so far is 5.2 T at 29 K [14]. To improve the trapped field, many factors have been used for PFM such as the environmental temperature, pulse duration time, amplitude of the external field, thermal conductivity of the bulk

[1] Authors to whom any correspondence should be addressed.

superconductor, the type of magnetizing coil(s) and so on [15–18]. In addition, some novel PFM techniques have been proposed such as sequential pulsed field application (SPA), an iteratively magnetizing pulsed field method with reduced amplitude (IMRA), a modified multi-pulsed technique with stepwise cooling (MMPSC) and so on [8, 14, 19, 20]. Apart from experiments, numerical simulation is a very useful tool for understanding the physical mechanism. Recently, the characteristics of trapped field in a bulk superconductor were studied numerically based on different numerical methods [16, 21–24].

Bulk superconductors (bulks) can trap a high field, but they are brittle materials and their mechanical strength is low. It is well known that bulks cannot withstand large mechanical loadings [25, 26]. When the superconductors are in a high field, they are subjected to a huge Lorentz force, which may damage them [10, 27]. During the manufacturing process, defects, microcracks and cavities may exist within the HTS and reduce the strength of a sample [28]. Much work has been done on the flux-pinning-induced magnetoelastic behaviors in superconductors. Ikuta *et al* found that magnetostriction in $Bi_2Sr_2CaCu_2O_8$ superconductors induced by flux pinning exceeds 10^{-4} at 4.8 K at first, and they also formulated pinning-induced deformation [29]. Then, the mechanical response of HTSs has received much attention. Ren *et al* observed the cracking of a superconducting disk with an environmental temperature of 49 K and a field-cooled condition of 14 T [26]. Nabialek *et al* investigated isotropic superconductors that have some special shapes, and then compared them with some experimental results [30]. Johansen investigated the flux-pinning-induced stress, strain and magnetostriction of type-II superconductors systematically [31–34]. In addition, the mechanical characteristics and crack problems were considered for HTS tape and cylindrical superconductors [35–43]. On the basis of previous investigations, a series of studies on the complicated structure and environment were presented [44–51]. Recently, Fujishiro *et al* investigated the stresses of REBaCuO superconducting ring bulks reinforced by a metal ring under FC magnetization, and they also investigated the total stress induced by electromagnetic stress plus thermal stress during the cooling down [27, 52]. Yang *et al* investigated the behavior of stress during PFM, where the superconductor is regarded as infinitely long [53]. The increase in temperature during PFM cannot be neglected and will cause a large thermal stress. However, the mechanical response of finite bulk superconductors under PFM has rarely been investigated.

In this paper, we consider the mechanical response of a cylindrical superconductor under electromagnetic stress and thermal stress during pulsed field magnetization. The effects of the peak value of the applied field and the size of bulk superconductors are studied. Due to the cylindrical symmetry, we can simplify the three-dimensional model to a 2D axisymmetric problem. Firstly, based on the H-formulation and the law of heat transfer, we can obtain the distributions of the electromagnetic field and the temperature field. After that, by using the dynamic equilibrium equations, the radial and hoop stresses caused by electromagnetic force and thermal strain are determined. The structure of this paper is as follows: in section 2, the model is established; in section 3, the trapped fields found from experimental results and numerical calculation are compared firstly, and then the trapped field and mechanical response under different conditions are presented and discussed. Finally, a summary and conclusion are drawn in section 4.

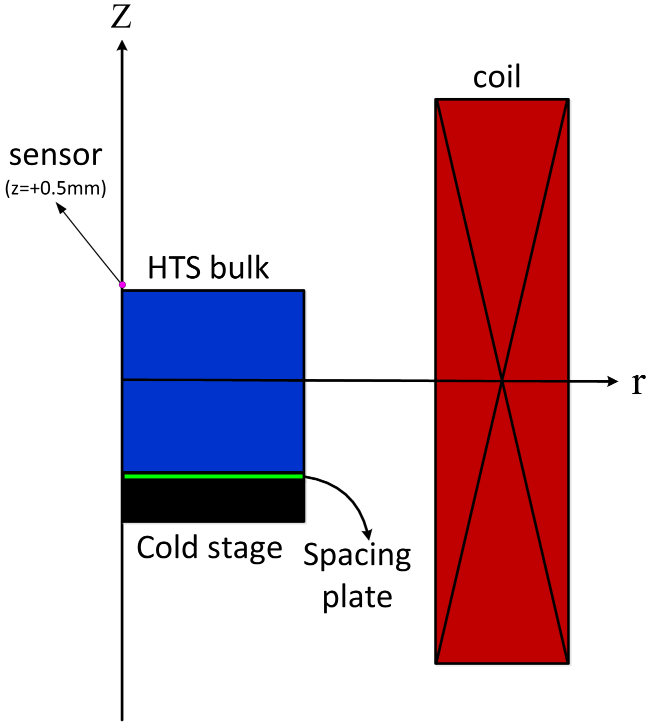

Figure 1. Schematic view of the experimental set-up for numerical simulation.

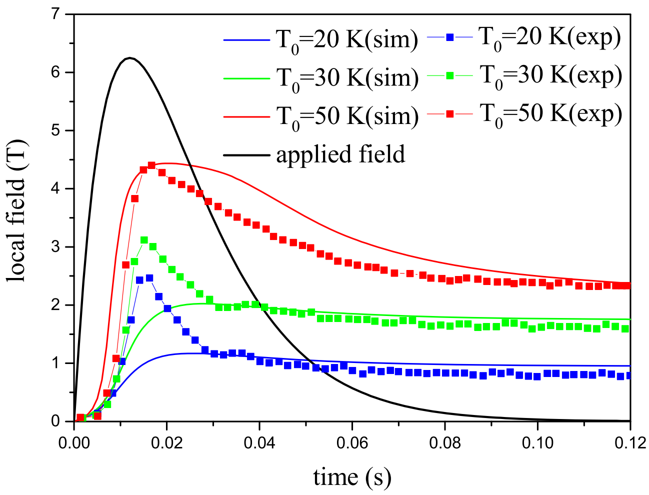

Figure 2. The time evolution of the trapped field for the PFM of $B_{max} = 6.25$ T at $T_0 = 20, 30, 50$ K.

2. Numerical model

2.1. Magnetic–thermal coupling

The numerical simulation is based on the experimental results [54]. The experiment set-up is described in [55] and a schematic view is shown in figure 1. The bulk superconductor is a

Table 1. Parameters used in the simulation of magnetic–thermal coupling [16, 59].

Symbol	Description	Values
E_c	characteristic electric field	1×10^{-6} V m^{-1}
ρ_{normal}	resistivity in the normal state of the sample	3.5×10^{-6} V A^{-1} m
α_1	critical current density extrapolated to $B = 0$ T and $T = 0$ K	4.6×10^8 A m^{-2}
n	value of n in equation (3)	8
B_0	fitting parameter in equation (6)	1.3 T
ρ_m	mass density of the sample	5900 kg m^{-3}
c	specific heat of the sample	132 J kg^{-1} K^{-1}
k_{ab}	thermal conductivity of the superconductor along the *ab* plane	20 W m^{-1} K^{-1}
k_c	thermal conductivity of the superconductor along the *c* direction	4 W m^{-1} K^{-1}
h	thickness of the sample	15 mm
d	diameter of the sample	46 mm
k_{sp}	thermal conductivity of the spacing plate	0.5 W m^{-1} K^{-1}
ρ_{sp}	mass density of the spacing plate	7310 kg m^{-3}
c_{sp}	specific heat of the spacing plate	150 J kg^{-1} K^{-1}
$B_{\max}$	peak value of the applied pulsed field	6.25 T
τ	rise time of the applied pulsed field	10 ms
T_c	critical temperature of the superconductor	92 K
T_0	initial temperature	30 K

sample of GdBCO, which is placed on the cold stage of a refrigerator in a vacuum chamber. From the schematic view, we can see that there is a spacing plate between the bulk and the cold stage, which ensures a good thermal contact between them [16]. The sensor is also indicated in the schematic view. The external applied magnetic field generated by a copper solenoid is parallel to the axial direction of the sample (z-axis). Due to the cylindrical symmetry, the three-dimensional problem can be simplified as a 2D axisymmetric case. Based on the H-formulation and the first law of thermodynamics, we analyze the distributions of electromagnetic field and temperature field.

When placed in the external magnetic field, the shielding current induced by the field will flow along the circular loop in the superconductor. The relation between the current density and magnetic field is

$$\nabla \times \mathbf{H} = \mathbf{J}. \tag{1}$$

Faraday's law is

$$\nabla \times \mathbf{E} + \frac{\partial \mathbf{B}}{\partial t} = 0. \tag{2}$$

The relationship between the electric field and current density is given by the power-law model [56]:

$$E = \rho_s J = E_c \left(\frac{J}{J_c}\right)^n \tag{3}$$

where ρ_s is the equivalent resistivity of the bulk superconductor. During the magnetization process, the normalized current density J/J_c can be much larger than 1 and its physical meaning is unreasonable [15]. Thus, the modified resistivity is adopted [57], which can be written as

$$\tilde{\rho} = \frac{\rho_s \cdot \rho_{normal}}{\rho_s + \rho_{normal}} \tag{4}$$

where ρ_{normal} represents the resistivity in the normal state.

Based on equations (1)–(4), we can get the governing equations for H-formulation in the 2D axisymmetric condition:

$$\begin{cases} \mu_0 \dfrac{\partial H_r}{\partial t} - \dfrac{1}{r} \dfrac{\partial [r\rho(\partial H_r/\partial z - \partial H_z/\partial r)]}{\partial z} = 0 \\ \mu_0 \dfrac{\partial H_z}{\partial t} + \dfrac{1}{r} \dfrac{\partial [r\rho(\partial H_r/\partial z - \partial H_z/\partial r)]}{\partial r} = 0 \end{cases} \tag{5}$$

where H_r, H_z represent the magnetic field components of $\mathbf{H}$ along r and z directions, respectively. E_c is the characteristic electric field and μ_0 is the permeability of vacuum.

With the experimental result, the critical current within the bulk sample can be described with the Kim model, which is expressed as follows [58]:

$$J_c(\mu_0 H) = \alpha_1 \left\{1 - \left(\frac{T}{T_c}\right)^2\right\}^{\frac{3}{2}} \frac{B_0}{|B| + B_0} \tag{6}$$

where α_1 is the critical current density at $B = 0$ T and $T = 0$ K, B_0 is the fitting parameter, which is a constant, and T_c is the critical temperature of the superconductor.

In the 2D axisymmetric model, the law of heat transfer can be described by [16]

$$\rho_m c \frac{\partial T}{\partial t} = \frac{1}{r}\frac{\partial}{\partial r}\left(r k_{ab} \frac{\partial T}{\partial r}\right) + \frac{\partial}{\partial z}\left(k_c \frac{\partial T}{\partial z}\right) + Q \tag{7}$$

where ρ_m and c represent the mass density and the specific heat of the sample, respectively. k_{ab}, k_c represent the thermal conductivity of the superconductor along the *ab* plane and c-axis, respectively. Q represents the heat source that is generated in the sample; it is calculated as the product of the electric field and current density, $Q = \mathbf{E} \cdot \mathbf{J}$.

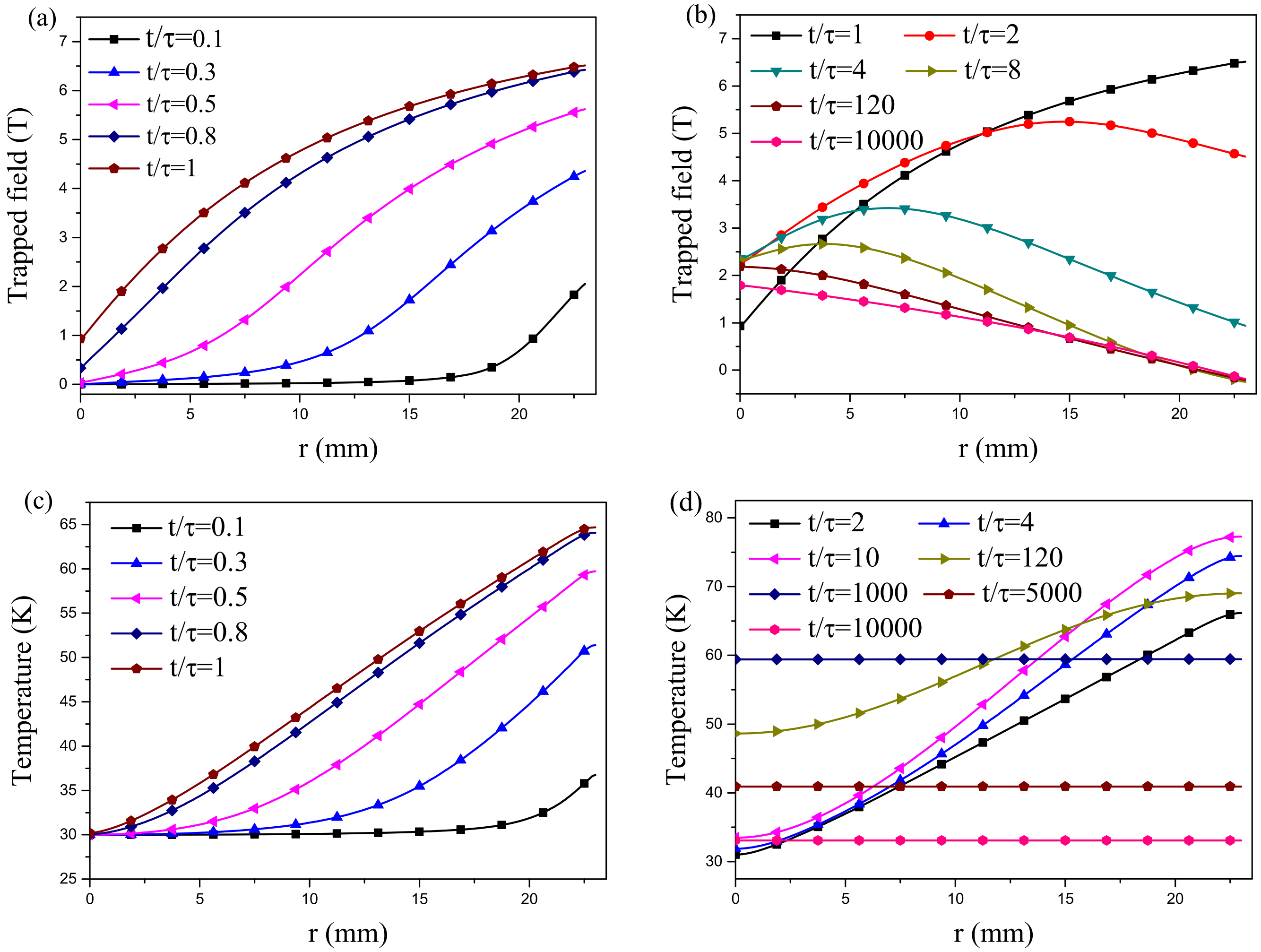

Figure 3. Time evolution of the trapped field distribution (a, b) and temperature distribution (c, d) at the surface of the bulk superconductor during the ascending stage (a, c) and the descending stage (b, d).

The applied pulsed field generated by the solenoid coil can be expressed as [59]

$$B_{ex}(t) = B_{\max}\frac{t}{\tau}\exp\left(1 - \frac{t}{\tau}\right) \tag{8}$$

where $B_{\max}$ and τ represent the peak value and the rise time of the applied pulsed field, respectively.

Using the commercial finite-element software COMSOL Multiphysics [60], we can obtain the distributions of the electromagnetic field and the temperature field with equations (5)–(8). Here, the PDE module and Heat Transfer in Solids module are adopted.

2.2. Numerical simulation of mechanical response

We can analyze the mechanical response by using the calculated distributions of electromagnetic field and temperature field in the bulk superconductor. When a magnetic field is trapped in superconductors, they are subjected to a Lorentz force that can be determined by

$$\mathbf{f} = \mathbf{J} \times \mathbf{B}. \tag{9}$$

To simplify the calculation, we consider the sample as an isotropic and linear elastic material. Since the electromagnetic stress and thermal stress will change with time, we consider the equilibrium equations, which contain the inertia forces

$$\begin{aligned} \frac{\partial\sigma_r}{\partial r} + \frac{\partial\tau_{zr}}{\partial z} + \frac{\sigma_r - \sigma_\varphi}{r} + f_r &= \rho_m\frac{\partial^2 u}{\partial t^2} \\ \frac{\partial\sigma_z}{\partial z} + \frac{\partial\tau_{rz}}{\partial r} + \frac{\tau_{rz}}{r} + f_z &= \rho_m\frac{\partial^2 w}{\partial t^2}. \end{aligned} \tag{10}$$

During the PFM, the thermal strain is not negligible and should also be considered. The relationship of the strains and the stresses can be written as

$$\begin{aligned} \varepsilon_r &= \frac{1}{\tilde{E}}[\sigma_r - \nu(\sigma_\varphi + \sigma_z)] + \alpha(T - T_0) \\ \varepsilon_\varphi &= \frac{1}{\tilde{E}}[\sigma_\varphi - \nu(\sigma_z + \sigma_r)] + \alpha(T - T_0) \\ \varepsilon_z &= \frac{1}{\tilde{E}}[\sigma_z - \nu(\sigma_r + \sigma_\varphi)] + \alpha(T - T_0) \\ \gamma_{zr} &= \frac{1}{G}\tau_{zr} = \frac{2(1 + \nu)}{\tilde{E}}\tau_{zr} \end{aligned} \tag{11}$$

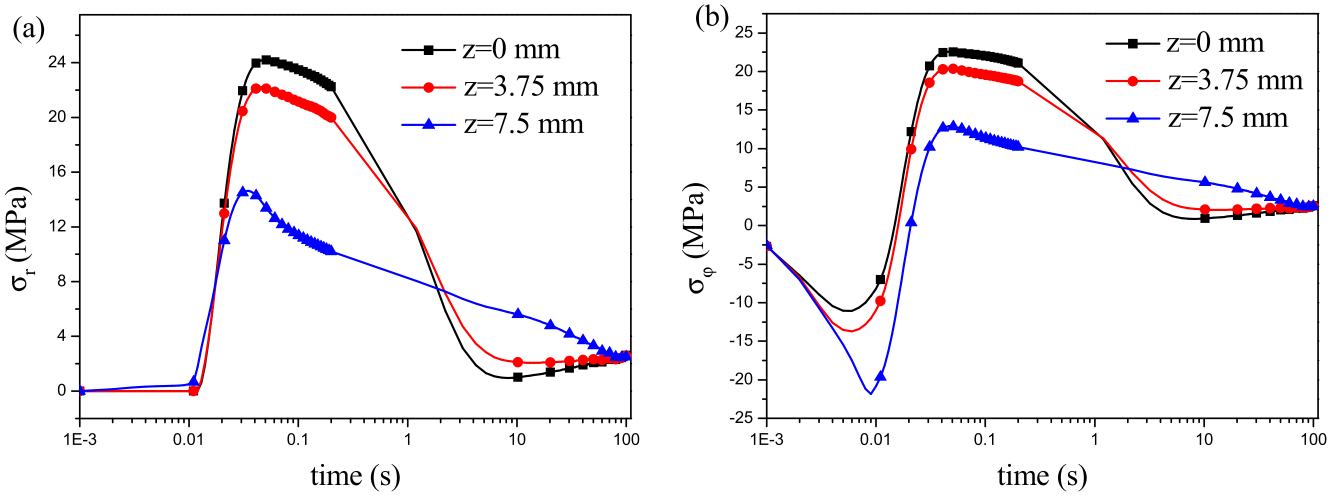

Figure 4. Results of the maximum radial stress (a) and maximum hoop stress (b) at $z = 0$ mm, $z = 3.75$ mm and $z = 7.5$ mm.

where f_r, f_z represent the Lorentz force components of $\boldsymbol{f}$ along r and z directions, respectively. $\tilde{E}$ is Young's modulus and ν is Poisson's ratio. T_0 represents the initial temperature and α is the thermal expansion coefficient. u and w represent the displacements along the r and z directions, respectively.

The 2D axisymmetric model based on the isotropic and linear elastic assumption is implemented in COMSOL Multiphysics. Based on equations (9)–(11), the mechanical response of the bulk superconductor can be obtained.

Table 2. Parameters used in the simulation of mechanical response [27, 62].

Symbol	Description	Values
$\tilde{E}$	Young's modulus of the sample	103 GPa
ν	Poisson's ratio of the sample	0.3
α	thermal expansion coefficient of the sample	1×10^{-5} K^{-1}
$\tilde{E}_{SUS}$	Young's modulus of the metal ring	193 GPa
ν_{SUS}	Poisson's ratio of the metal ring	0.28
α_{SUS}	thermal expansion coefficient of the metal ring	1.27×10^{-5} K^{-1}

3. Numerical results and discussions

3.1. Verification of results

In order to verify the accuracy of numerical simulation, we compare the numerical results of trapped field with experimental results [54] (see figure 2). In figure 2, the time evolution of the trapped field by numerical simulation is compared with experimental results, where the bulk GdBCO sample is 45 mm in diameter and 18 mm thick. The peak value and the rise time of the applied pulsed field are 6.25 T and 12 ms, respectively. The other parameters are from the references [16, 54]. We find that the two curves are very close except for the maximum value of the field. The difference in the peak values may be due to the fact that the thermal conductivity and specific heat will change with temperature. In addition, the inhomogeneity of the bulk may also affect the peak value of trapped field. Next we will analyze the trapped field and temperature distributions during PFM.

3.2. Trapped field and the temperature distributions during the PFM

Consider the bulk GdBCO sample, which is 46 mm in diameter and 15 mm thick. The rise time of the applied pulsed field is 10 ms and the environmental temperature is 30 K. The other parameters used for magnetic–thermal coupling and mechanical response are presented in tables 1 and 2, respectively. Firstly, we investigate the magnetic field and temperature distributions in the bulk superconductor. Figures 3(a)–(d) shows the trapped field and the temperature field distributions at the surface of the bulk superconductor during the PFM. The trends are consistent with reference [16]. From those it can be found that the magnetic flux penetrates into the superconductor from its boundary and that heat will also be generated at the boundary. Due to the heat conduction at the boundary, the thermal diffusion propagates more slowly than the magnetic flux. The final trapped field at the surface of the bulk superconductor was 1.79 T in the steady state. As the magnetic field is applied, the maximum temperature rise is about 47 K, which will have a dramatic effect on the stress distribution.

3.3. Radial stress and hoop stress distributions during the PFM

In order to study the mechanical response of the bulk superconductor, figures 4(a) and (b) show the results of the evolution of the maximum radial and hoop stresses with time for three planes of the bulk: $z = 0$ mm, $z = 3.75$ mm and $z = 7.5$ mm. The stress along the z direction is small, so we consider only the radial and hoop stresses. Since the bulk superconductors are brittle and their mechanical strength is low, the tensile stress is more important during the PFM. From figure 4, we can find that the maximum radial stress first

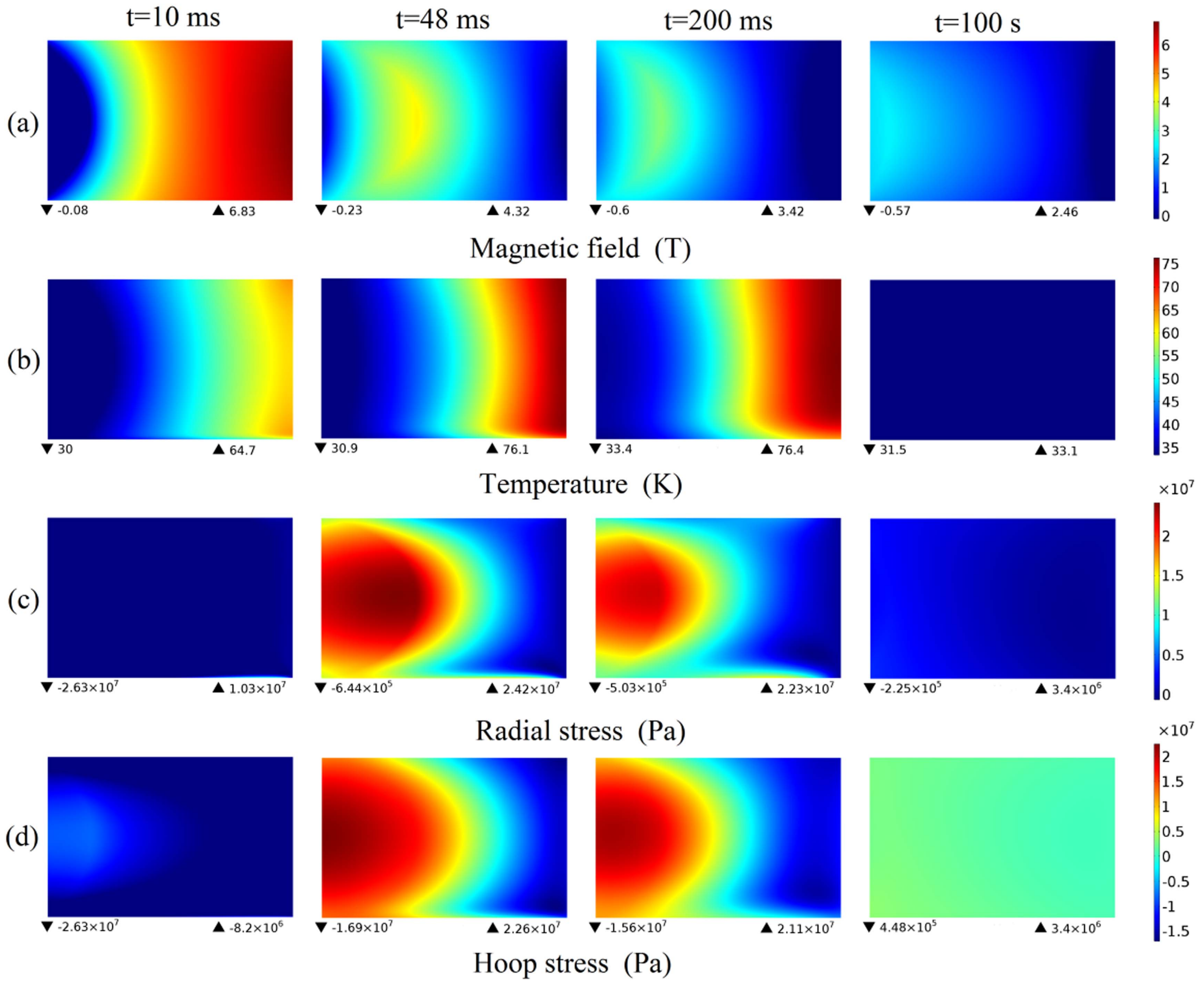

Figure 5. Distributions of magnetic field (a), temperature (b), radial stress (c) and hoop stress (d) at 10 ms, 48 ms, 200 ms and 100 s.

increases and then decreases, and the peak value of radial stress appears in the plane of $z = 0$ mm. The trend is similar for the hoop stress. This indicates that cracking is most likely to occur in the central plane ($z = 0$ mm). The maximum radial stress is about 24.2 MPa at 49 ms, and the maximum hoop stress is about 22.6 MPa at 46 ms. In order to present the evolution process, we plot the magnetic field, the temperature, the radial stress and the hoop stress distributions at 10 ms, 48 ms, 200 ms, 100 s in figure 5. It should be noted that the maximum radial stress is located in the region of maximum trapped field, which can be seen at 48 ms and 200 ms, and the maximum hoop stress appears in the center. The applied field achieves the peak values at 10 ms, while the temperature does not reach the peak value. Then, the radial and hoop stresses are still smaller. For the long-time relaxation (100 s), the trapped field distribution is stable and the temperature distribution is consistent with the environmental temperature, so the radial and hoop stresses are also small. It is to be noted that the thermal conductivity and specific heat are temperature-dependent. During the PFM process, a large temperature rise will lead to a change in thermal parameters. For simplicity, we assume that the thermal conductivity and the specific heat are temperature-independent in the simulation. Compared to the temperature-dependent parameters, the constant thermal conductivity and specific heat that we used can lead to differences in trapped field, temperature rise and mechanical stress. However, the difference in the maximal stress is relatively small.

It is to be noted that both the electromagnetic force and thermal stress contribute to the total stress, and we will consider the effects of these separately. Here, only the radial stress and the hoop stress distributions at the $z = 0$ mm plane are presented. Figures 6(a)–(d) show the trapped field and the temperature distributions. Comparing with figure 3, we can find that the penetration depth at the surface is larger than in the central plane, and the behavior of thermal diffusion is also similar. In addition, the final trapped field in the central plane is 2.30 T in the steady state, which is higher than at the surface. However, the maximum temperature at the boundary is nearly the same. Figures 7(a) and (b) show the time dependence of the total radial stress distribution during the ascending and descending stages, respectively. In figure 7(a),

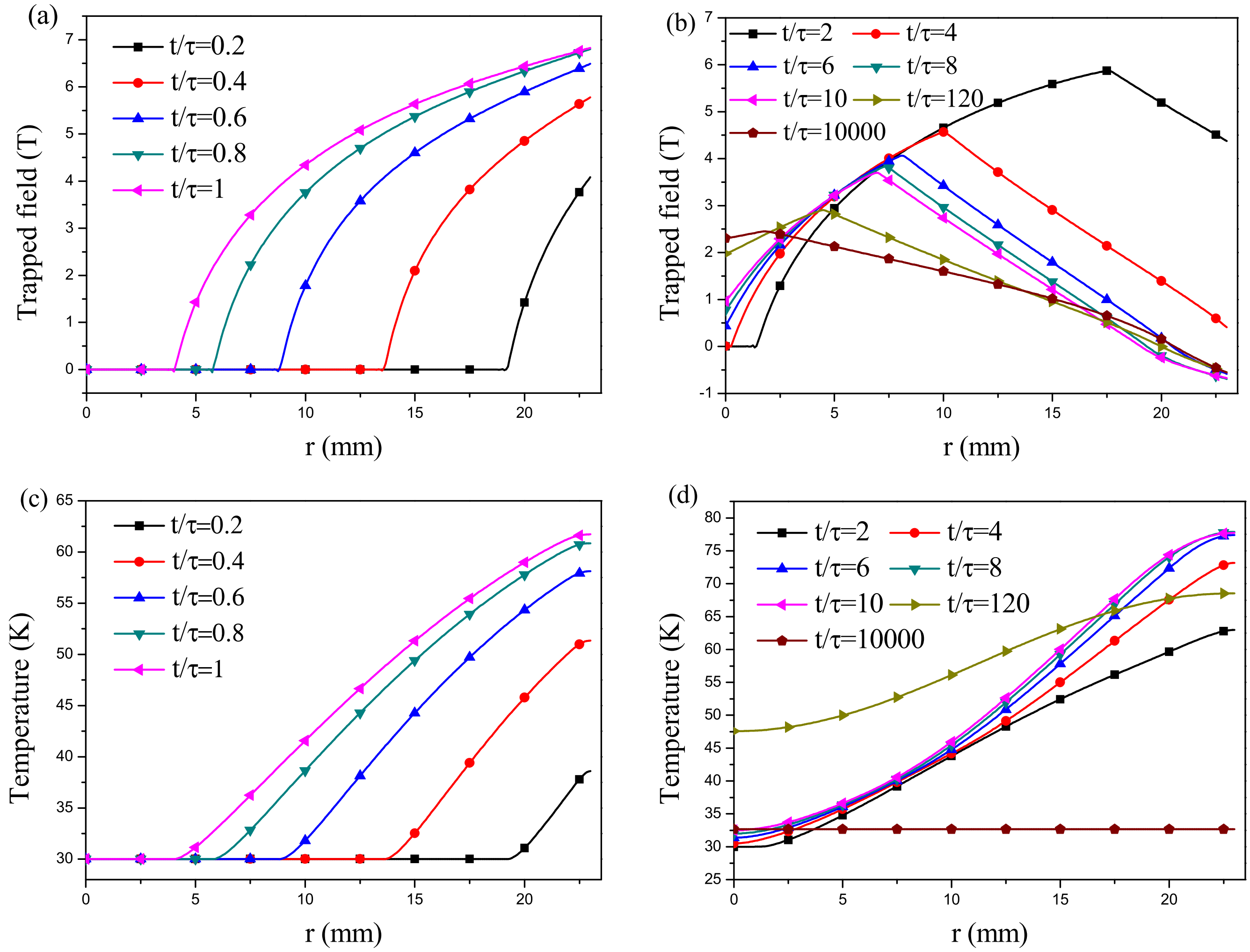

Figure 6. The distributions of trapped field (a, b) and temperature (c, d) along the $z = 0$ mm plane during the ascending stage (a, c) and the descending stage (b, d).

the magnetic flux penetrates into the superconductor, which generates the compressive stress. During the descending stage, the compressive stress changes to tensile stress. In figure 7(b), the total radial stress increases at first and then decreases as the applied field decreases. The maximum of total radial stress is 24.2 MPa at $r = 7$ mm, where the cracking is most likely to occur. Figures 7(c) and (d) show the radial electromagnetic stress distribution during the PFM. As we know, during the ascending stage the radial stress is compressive. The Lorentz body force will change direction during the descending stage and the radial stress will become tensile. The maximum radial stress is about 11.8 MPa, which is smaller than the maximum total radial stress. Figures 7(e) and (f) show the radial thermal stress distribution. For the PFM, the temperature will increase due to the motion of flux, and the maximum radial thermal stress is about 20.2 MPa. From figure 7, it can be found that the thermal stress will significantly increase the total stress. This trend is a little different from the results given in reference [53], which is mainly due to the difference in material parameters adopted. Figure 8 shows the hoop stress distribution during the ascending and descending stages. The trend of variation is generally similar to that of radial stress. Furthermore, the position of maximal hoop stress is at $r = 0$ mm, which is different from the radial stress. With increasing time, the temperature in the bulk will return to the environmental temperature. Then, the stress caused by thermal strain gradually decreases, so the total radial stress and the total hoop stress also decrease and finally become equal to the electromagnetic stress.

In our simulation, the metal ring fitting is neglected to simplify the computation. Since the metal ring and bulk have different thermal expansion coefficients, the residual stress will appear during the cooling down from room temperature (300 K) to operating temperature (30 K). Figure 9 shows maps of the radial and hoop residual stresses in the bulk, where the thickness of the metal ring fitting is 5 mm. The distribution of hoop stress is similar to the results given in [27]. It can be found that the maximum of radial residual stress at the surface of the bulk is about 32.3 MPa. Since the locations of peak values of stresses (residual stress, thermal stress and electromagnetic stress) are different, the total stress is still smaller than the fracture strength.

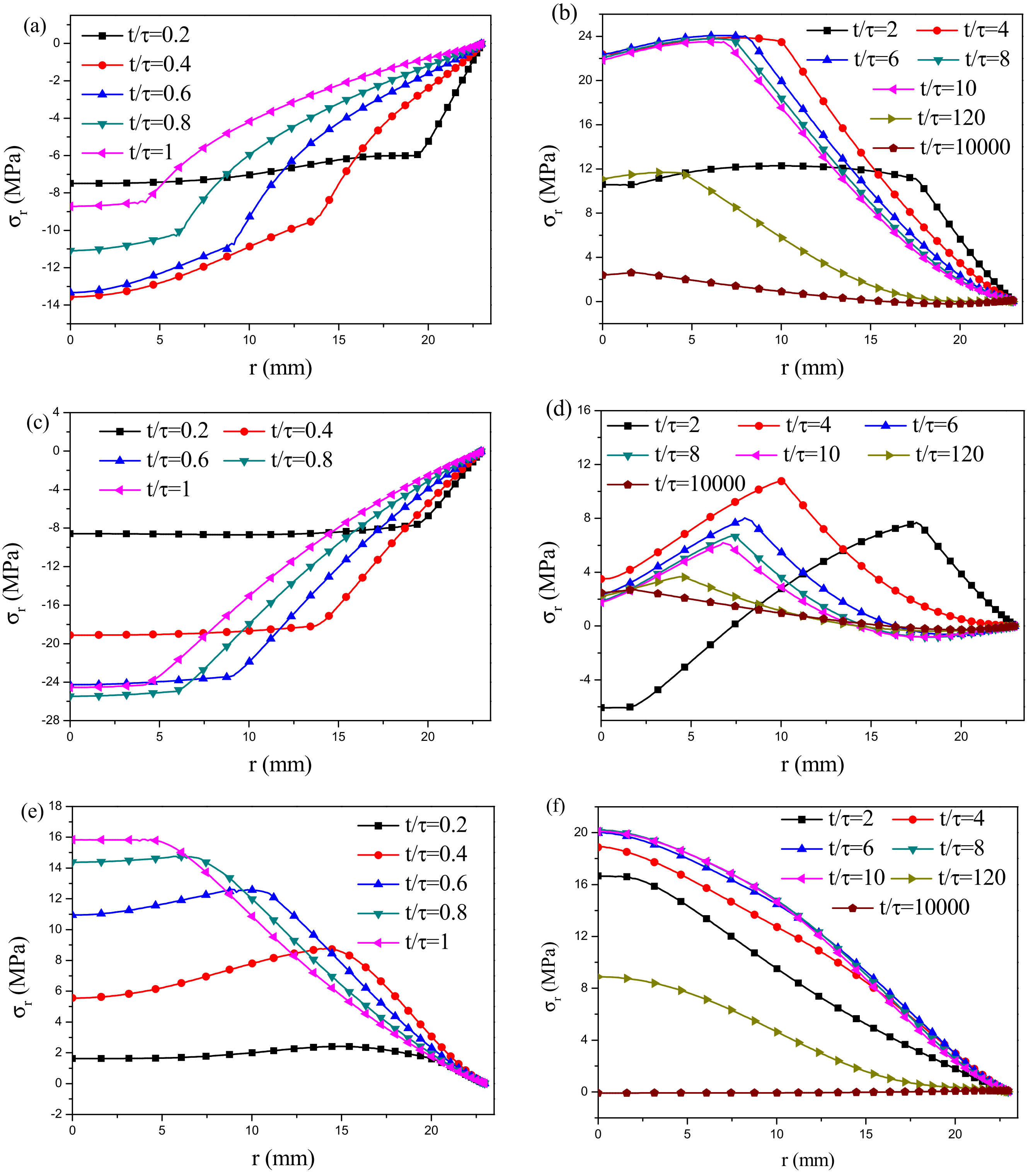

Figure 7. The time dependences of the distributions of total radial stress (a), (b), electromagnetic radial stress (c), (d), and radial thermal stress (e), (f) along the $z = 0$ mm plane during the ascending and descending stages, respectively.

3.4. Influences of the applied field and the size of the sample

With increasing peak value of the applied field, the trapped field will first increase and then decrease [16]. This is because a larger field can cause a large temperature rise that will reduce the critical current density so that the trapped field will be decreased. Figure 10 shows the distribution of the total maximum radial and hoop stresses along the $z = 0$ mm plane for different applied fields. With increasing peak value of the applied field, the maximum radial stress also increases and the position of maximal radial stress moves from the boundary towards the center. In figure 10(b), the maximal hoop stress increases monotonically with increasing peak value of the

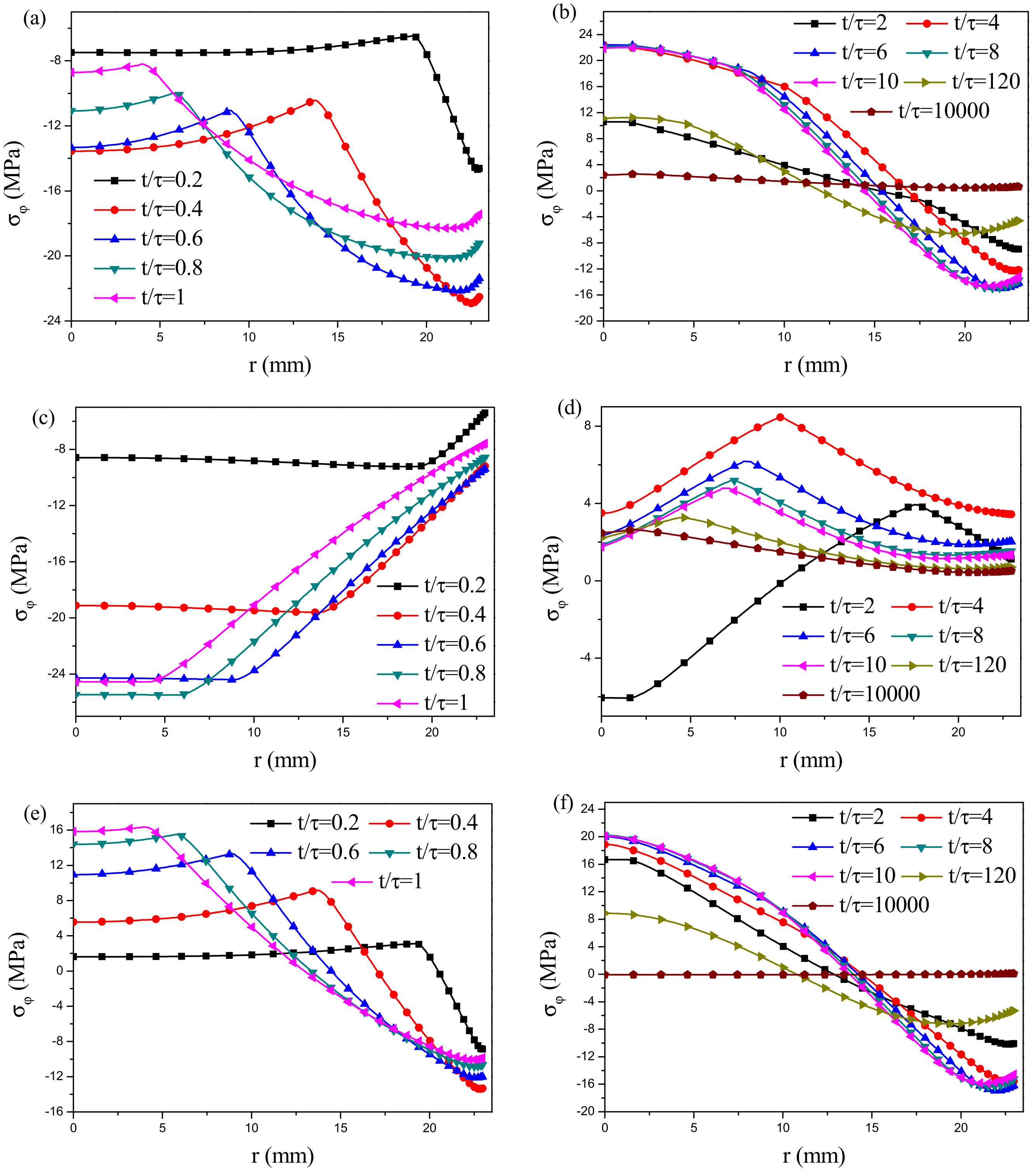

Figure 8. The time dependences of the distributions of total hoop stress (a), (b), electromagnetic hoop stress (c), (d), and hoop thermal stress (e), (f) along the $z = 0$ mm plane during the ascending and descending stages, respectively.

applied field, and the position of maximal hoop stress appears in the center.

From figure 10, we can find that both the maximal radial and hoop stresses are about 41.84 MPa. The peak values of radial and hoop stresses are located in the center of the bulk, and cracking is most likely to occur there. The peak value is smaller than the fracture strength, which is about 50 MPa [27, 52]. However, as the applied magnetic field is larger, the peak value may exceed the strength. In addition, during the manufacturing process, the bulk may contain defects, micro-cracks and cavities, which can cause stress concentration and damage to the bulk [28, 32].

In figures 11 and 12 we analyze the effect of the size of bulk superconductors. Figure 11 shows the effect of the

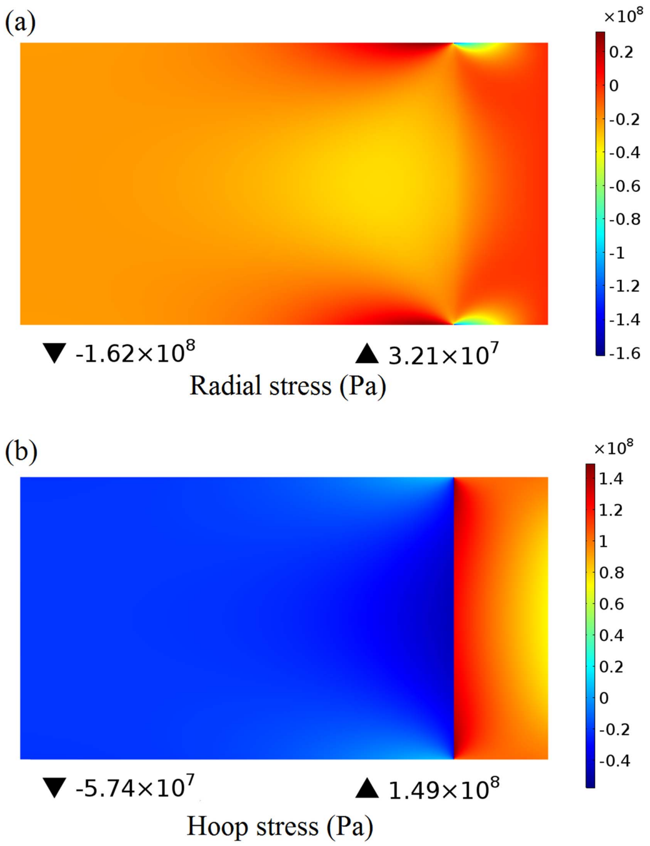

Figure 9. Maps of the radial (a) and hoop (b) residual stresses in the bulk.

thickness of bulk superconductors of the same diameter. With increasing thickness, the trapped field will first increase and then decrease. When the thickness is smaller, the magnetic flux penetrates into the superconductor easily, and the maximum total stress is almost equal to the maximum thermal stress plus the maximum electromagnetic stress. Thus, the maximum radial stress and the hoop stress decrease with the thickness of the bulk. When the bulk is thick enough, it is difficult for the magnetic flux to penetrate into the superconductor under the same applied magnetic field. The final trapped field is smaller, and the maximum radial and hoop stresses would also decrease. Figure 12 shows the effect of the diameter of bulk superconductors with the same thickness. Unlike with the thickness, the total maximal stress increases monotonically with the radius due to the larger temperature rise. It is interesting that the effects of thickness and radius on the maximal stress are different. For bulk superconductors with same diameter, the penetration of magnetic flux becomes easier with the decreasing thickness, and the maximal electromagnetic stress also increases with the decreasing thickness. Since the thermal stress is close for different thicknesses, a smaller thickness corresponds to a larger maximal total stress. For bulk superconductors with the same thickness, the penetration of magnetic flux becomes easier with increasing radius. In other words, increasing radius is equivalent to decreasing thickness. In addition, the thermal stress increases with the radius. Thus, a larger radius leads to a larger maximal stress.

3.5. Influence of different PFM techniques

To investigate the effect of multi-pulsing, three PFM techniques have been studied in this section [61], where the size and environmental temperature are the same as given in section 3.2. By adopting SPA, figure 13 shows the time evolutions of the trapped field and the temperature distribution of the central point on the top surface. Three identical sequential pulsed fields of amplitude $B_{\max} = 6.25$ T are applied. Figure 13(a) shows that the trapped field increases with the number of pulses; however, the increment in the trapped field is decreasing; figure 13(b) shows that the temperature rise decreases for PFM, which agrees well with the experimental results [9]. Thus, SPA is an effective method for improving the trapped field. The time evolution of the total maximum stress along the $z = 0$ mm plane is presented in figure 14. From that we can find that the maximum radial stress increases slightly and the maximum hoop stress decreases slightly. The maximum radial stress is about 24.94 MPa. Then, the iteratively magnetizing pulsed field method with reduced amplitude (IMRA) is analyzed in figures 15 and 16, where the iteratively applied pulsed field amplitudes are 6.25 T, 5.6 T and 5 T. The trend of variation in figure 15(a) is the same as in figure 13(a), and the trapped field will also increase slightly. With decreasing amplitude of the iteratively pulsed field, the rise in temperature obviously decreases, so that the stress in figure 16 also decreases. Finally, the results for the iteratively magnetizing pulsed field method with increased amplitude are presented, where the iteratively applied pulsed field amplitudes are 6.25 T, 7 T and 7.6 T. Figure 17(a) shows that the trapped field decreases with the multi-pulsed field; this is because the increasing rise in temperature will reduce the critical current density; figure 17(b) shows the time evolution of the temperature distribution of the central point on the top surface during the magnetization process. By considering the increase in temperature, the radial stress and the hoop stress will also increase (figure 18); the maximum radial stress is about 31.87 MPa and the maximum hoop stress is about 29.76 MPa.

4. Conclusion

In this paper, numerical simulations of the trapped field and stress distributions in bulk superconductors during pulsed field magnetization were presented. Considering the cylindrical symmetry, we simplified the three-dimensional model to a 2D axisymmetric model. Based on the H-formulation and the law of heat transfer, we can obtain the trapped field and the temperature distributions. Then, after solving the dynamic equilibrium equations, the mechanical response of the superconductor caused by electromagnetic force and thermal strain was studied. During the PFM, the thermal strain has a significant effect on the total stress. The effects of the peak value of the applied field and the size of the bulk

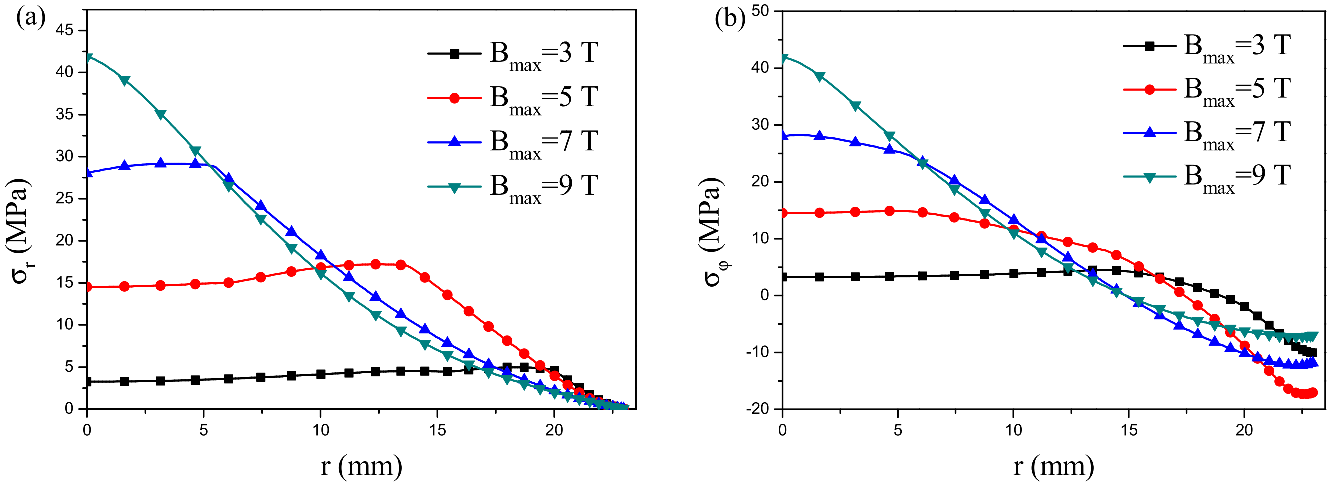

Figure 10. The effects of the peak value of the applied field: distributions of the total maximum radial (a) and hoop (b) stress along the $z = 0$ mm plane for different applied fields.

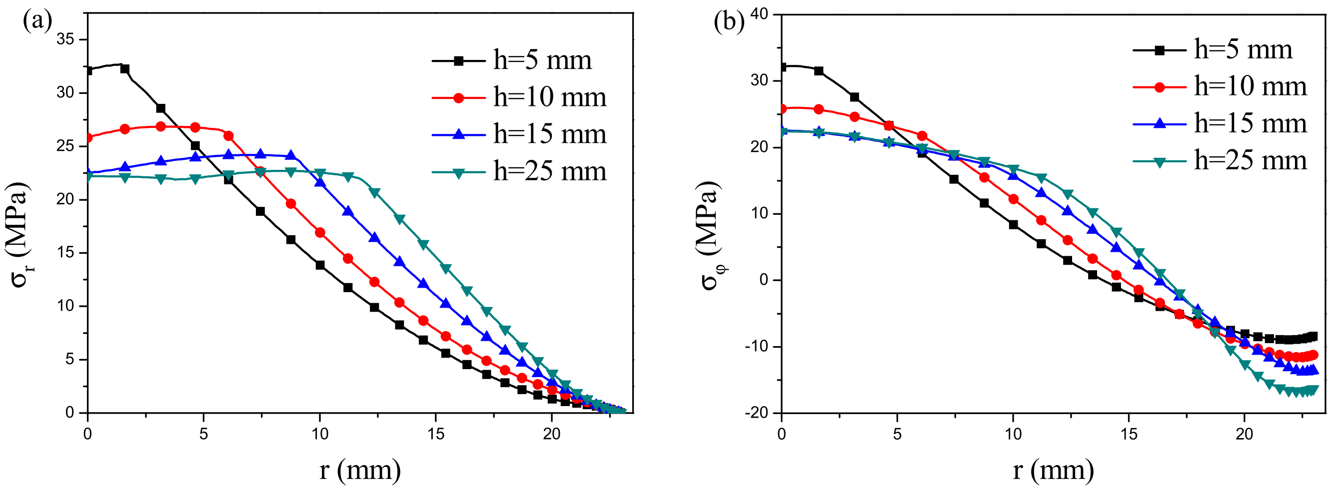

Figure 11. The effect of the thickness of bulk superconductors with the same diameter: distributions of the total maximum radial (a) and hoop (b) stress along the $z = 0$ mm plane.

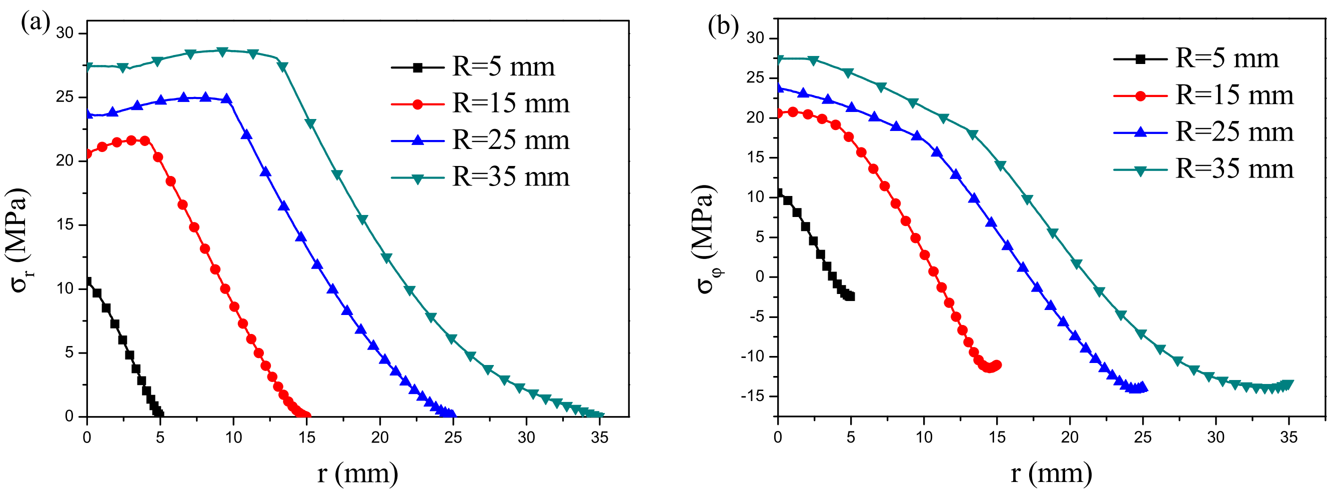

Figure 12. The effect of the diameter of bulk superconductors with the same thickness: distributions of the total maximum radial (a) and hoop (b) stress along the $z = 0$ mm plane.

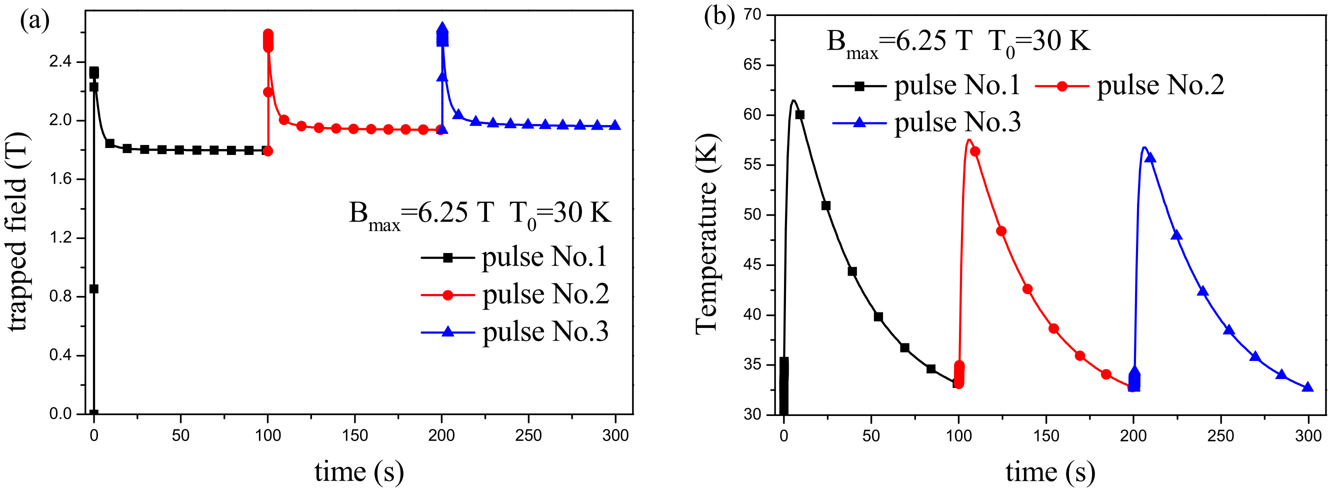

Figure 13. Time evolution of the trapped field (a) and the temperature distribution (b) of the central point on the top surface during the iteratively pulsed field magnetization with identical amplitude.

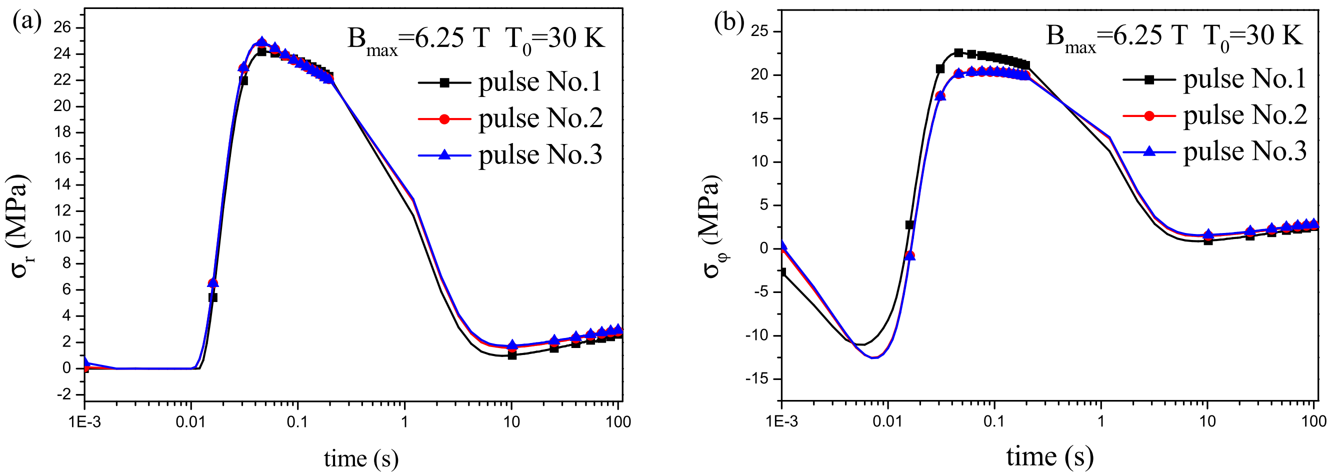

Figure 14. Time evolution of the total maximum radial (a) and hoop (b) stresses along the $z = 0$ mm plane during the iteratively pulsed field magnetization with identical amplitude.

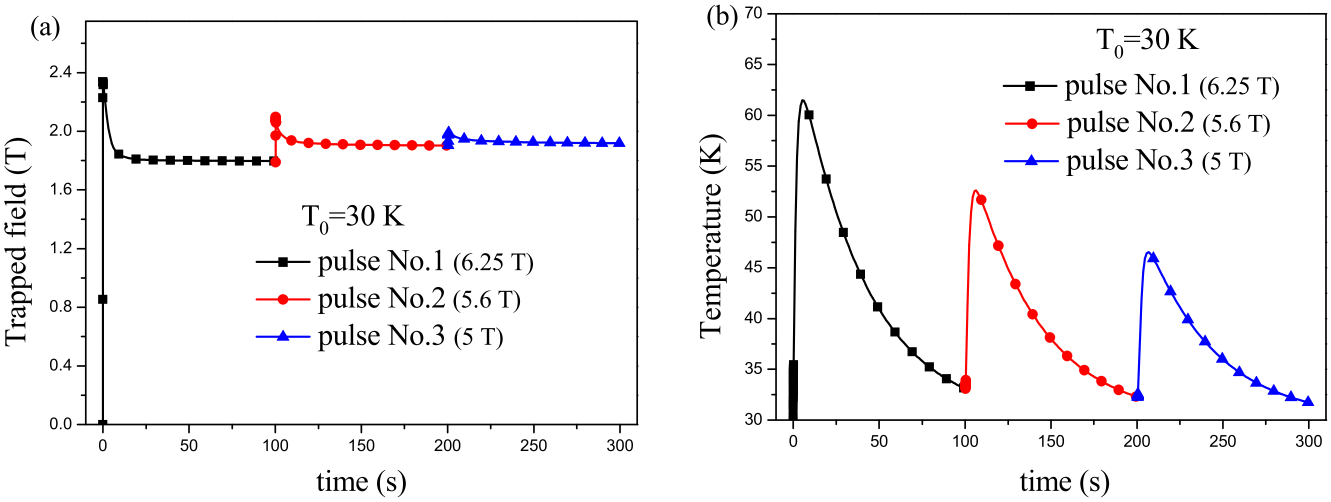

Figure 15. Time evolution of the trapped field (a) and the temperature distribution (b) of the central point on the top surface during the iteratively pulsed field magnetization with reduced amplitude.

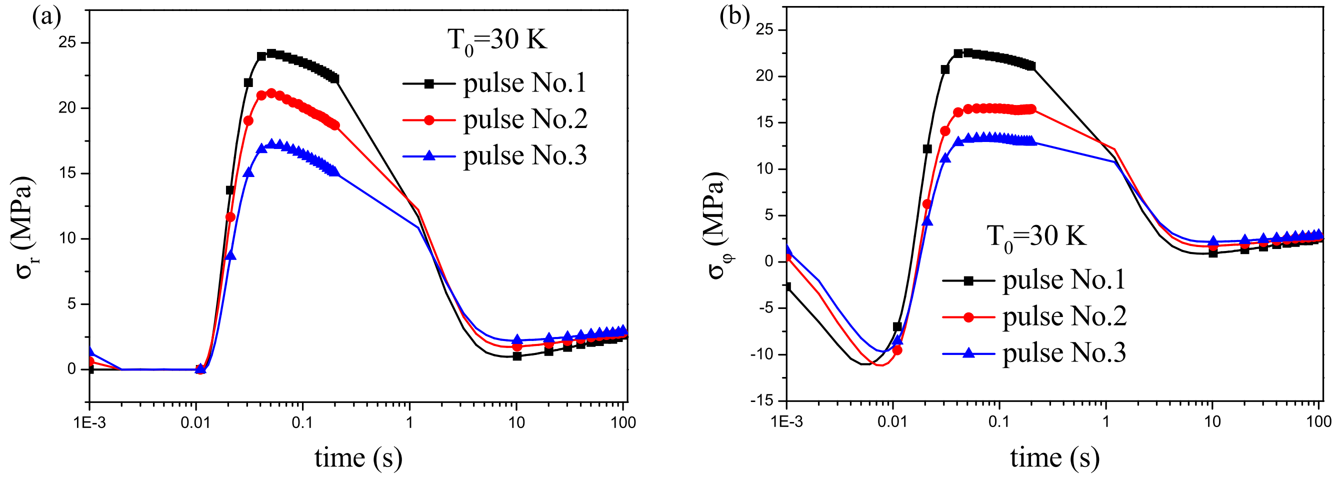

Figure 16. Time evolution of the total maximum radial (a) and hoop (b) stresses along the $z = 0$ mm plane during the iteratively pulsed field magnetization with reduced amplitude.

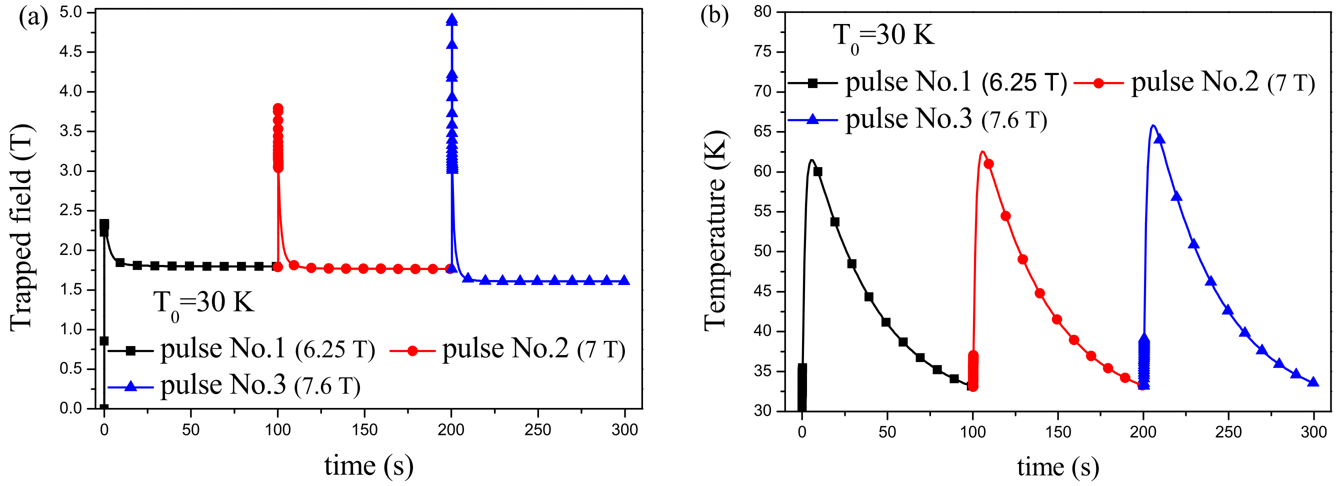

Figure 17. Time evolution of the trapped field (a) and the temperature distribution (b) of the central point on the top surface during the iteratively pulsed field magnetization with increasing amplitude.

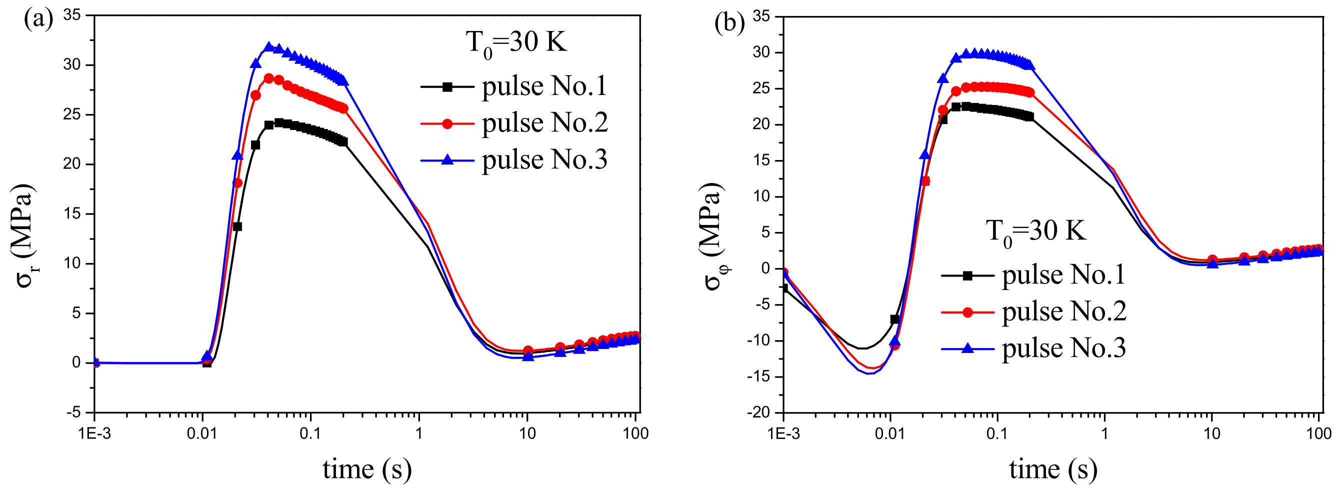

Figure 18. Time evolution of the total maximum radial (a) and hoop (b) stresses along the $z = 0$ mm plane during the iteratively pulsed field magnetization with increasing amplitude.

superconductors have also been considered. With increasing applied field, the trapped field first increases and then decreases, and both the radial and hoop stresses increase monotonically. With increasing thickness, the trapped field first increases and then decreases, and the maximum radial and hoop stresses decrease. In addition, the trends of maximum radial and hoop stresses with the radius are opposite to those with the thickness. After that, three different multi-pulsed magnetization methods have been studied and the results are qualitatively consistent with experiment.

Acknowledgments

The authors acknowledge the supports from the National Natural Science Foundation of China (Nos 11472120 and 11421062), the National Key Project of Scientific Instrument and Equipment Development (11327802) and the Fundamental Research Funds for the Central Universities (lzujbky-2017-k18).

ORCID iDs

Huadong Yong https://orcid.org/0000-0002-0304-3191

References

[1] Murakami M 2000 Progress in applications of bulk high temperature superconductors *Supercond. Sci. Technol.* **13** 448–50
[2] Hull J R and Murakami M 2004 Applications of bulk high-temperature superconductors *Proc. IEEE* **92** 1705–18
[3] Krabbes G, Fuchs G, Canders W R, May H and Palka R 2006 *High Temperature Superconductor Bulk Materials: Fundamentals, Processing, Properties Control, Application Aspects* (Weinheim: Wiley) p 106
[4] Murakami M 2007 Processing and applications of bulk RE–Ba–Cu–O superconductors *Int. J. Appl. Ceram. Technol.* **4** 225–41
[5] Zhou D, Izumi M, Miki M, Felder B, Ida T and Kitano M 2012 An overview of rotating machine systems with high-temperature bulk superconductors *Supercond. Sci. Technol.* **25** 7230–5
[6] Yokoyama K, Oka T, Okada H, Fujine Y, Chiba A and Noto K 2003 Solid–liquid magnetic separation using bulk superconducting magnets *IEEE Trans. Appl. Supercond.* **13** 1592–5
[7] Nakamura T, Tamada D, Yanagi Y, Itoh Y, Nemoto T, Utumi H and Kose K 2015 Development of a superconducting bulk magnet for NMR and MRI *J. Magn. Reson.* **259** 68–75
[8] Zou J, Ainslie M D, Fujishiro H, Bhagurkar A G, Naito T, Babu N H, Fagnard J, Vanderbemden P and Yamamoto A 2015 Numerical modelling and comparison of MgB_2 bulks fabricated by HIP and infiltration growth *Supercond. Sci. Technol.* **28** 075009
[9] Ainslie M D and Fujishiro H 2015 Modelling of bulk superconductor magnetization *Supercond. Sci. Technol.* **28** 053002
[10] Durrell J H, Dennis A R, Jaroszynski J, Ainslie M D, Palmer K G, Shi Y, Campbell A M, Hull J, Strasik M and Hellstrom E 2014 A trapped field of 17.6 T in melt-processed, bulk Gd–Ba–Cu–O reinforced with shrink-fit steel *Supercond. Sci. Technol.* **27** 082001
[11] Fujishiro H, Naito T and Furuta D 2011 Analysis of temperature and magnetic field distribution in superconducting bulk during pulsed field magnetization *IEEE Trans. Appl. Supercond.* **21** 2723–6
[12] Fujishiro H, Hiyama T, Naito T, Yanagi Y and Itoh Y 2009 Enhancement of trapped field and total trapped flux on GdBaCuO bulk by the MMPSC + IMRA method *Supercond. Sci. Technol.* **22** 095006
[13] Ainslie M D, Fujishiro H, Ujiie T, Zou J, Dennis A R, Shi Y H and Cardwell D A 2014 Modelling and comparison of trapped fields in (RE)BCO bulk superconductors for activation using pulsed field magnetization *Supercond. Sci. Technol.* **27** 065008
[14] Fujishiro H, Tateiwa T, Fujiwara A, Oka T and Hayashi H 2006 Higher trapped field over 5 T on HTSC bulk by modified pulse field magnetizing *Physica* C **445–448** 334–8
[15] Zou S, Zermeño V M R and Grilli F 2015 Simulation of high temperature superconducting bulks magnetized by pulsed field magnetization with an electromagnetic–thermal coupled model (arXiv:1511.00516)
[16] Fujishiro H and Naito T 2010 Simulation of temperature and magnetic field distribution in superconducting bulk during pulsed field magnetization *Supercond. Sci. Technol.* **23** 105021
[17] Ida T, Sakashita H, Okuda H and Izumi M 2008 Trapped field measurements of Gd–Ba–Cu–O bulk superconductor in controlled pulse field magnetizing *J. Phys.: Conf. Ser.* **97** 012292
[18] Ida T, Matsuzaki H, Akita Y, Izumi M, Sugimoto H, Hondou Y, Kimura Y, Sakai N, Nariki S and Hirabayashi I 2004 Magnetization properties for Gd–Ba–Cu–O bulk superconductors with a couple of pulsed-field vortex-type coils *Physica* C **412–414** 638–45
[19] Fujishiro H, Yokoyama K, Kaneyama M, Oka T and Noto K 2004 Estimation of generated heat in pulse field magnetizing for SmBaCuO bulk superconductor *Physica* C **412** 646–50
[20] Yanagi Y, Itoh Y, Yoshikawa M, Oka T, Hosokawa T, Ishihara H, Ikuta H and Mizutani U 2000 Trapped field distribution on Sm–Ba–Cu–O bulk superconductor by pulsed-field magnetization *Advances in Superconductivity* vol 12 (Tokyo: Springer) p 470
[21] Shen Z, Ainslie M D, Campbell A M and Cardwell D A 2015 Computation of the field in an axial gap, trapped-flux type superconducting electric machine *IEEE Trans. Appl. Supercond.* **25** 5201005
[22] Grilli F, Pardo E, Stenvall A, Nguyen D N, Yuan W and Gomory F 2013 Computation of losses in HTS under the action of varying magnetic fields and currents *IEEE Trans. Appl. Supercond.* **24** 78–110
[23] Campbell A M 2011 An introduction to numerical methods in superconductors *J. Supercond. Nov. Magn.* **24** 27–33
[24] Patel A and Glowacki B A 2012 Enhanced trapped field achieved in a superconducting bulk using high thermal conductivity structures following simulated pulsed field magnetization *Supercond. Sci. Technol.* **25** 125015
[25] Gruss S, Fuchs G, Krabbes G, Verges P, Stöver G, Müller K-H, Fink J and Schultz L 2001 Superconducting bulk magnets: very high trapped fields and cracking *Appl. Phys. Lett.* **79** 3131
[26] Ren Y, Weinstein R, Liu J, Sawh R and Foster C 1995 Damage caused by magnetic pressure at high trapped field in quasi-permanent magnets composed of melt-textured YBaCuO superconductor *Physica* C **251** 15–26
[27] Takahashi K, Fujishiro H, Naito T, Yanagi Y, Itoh Y and Nakamura T 2017 Fracture behavior analysis of EuBaCuO superconducting ring bulk reinforced by a stainless steel ring

during field-cooled magnetization *Supercond. Sci. Technol.* **30** 115006
[28] Diko P, Krabbes G and Wende C 2001 Influence of Ag addition on crystallization and microstructure of melt-grown single-grain $YBa_2Cu_3O_7$ bulk superconductors *Supercond. Sci. Technol.* **14** 486–95
[29] Ikuta H, Hirota N, Nakayama Y, Kishio K and Kitazawa K 1993 Giant magnetostriction in $Bi_2Sr_2CaCu_2O_8$ single crystal in the superconducting state and its mechanism *Phys. Rev. Lett.* **70** 2166
[30] Nabiałek A, Szymczak H, Sirenko V and D'yachenko A 1998 Influence of the real shape of a sample on the pinning induced magnetostriction *J. Appl. Phys.* **84** 3770
[31] Johansen T H 1999 Flux-pinning-induced stress and strain in superconductors: long rectangular slab *Phys. Rev.* B **59** 11187
[32] Johansen T H 1999 Flux-pinning-induced stress and strain in superconductors: Case of a long circular cylinder *Phys. Rev.* B **60** 9690
[33] Johansen T, Wang C, Chen Q and Chu W 2000 Enhancement of tensile stress near a hole in superconducting trapped-field magnets *J. Appl. Phys.* **88** 2730
[34] Johansen T H 2000 Flux-pinning-induced stress and magnetostriction in bulk superconductors *Supercond. Sci. Technol.* **13** R121
[35] Yong H and Zhou Y 2008 Kim model of stress induced by flux pinning in type-II superconductors *J. Appl. Phys.* **103** 113903
[36] Zeng J, Zhou Y H and Yong H D 2009 Kim model for stress distribution in a hollow cylindrical superconductor *Physica* C **469** 822–6
[37] Yong H and Zhou Y 2011 Stress distribution in a flat superconducting strip with transport current *J. Appl. Phys.* **109** 073902
[38] Gao Z, Zhou Y and Lee K Y 2010 Crack–inclusion problem for a long rectangular slab of superconductor under an electromagnetic force *Comput. Mater. Sci.* **50** 279–82
[39] Feng W, Zhang R and Ding H 2012 Crack problem for an inhomogeneous orthotropic superconducting slab under an electromagnetic force *Physica* C **477** 32–5
[40] Yong H and Zhou Y 2013 Flux pinning induced stress and magnetostriction in a long elliptic cylindrical superconductor *J. Appl. Phys.* **114** 023902
[41] Yong H, Lu Y, Jing Z and Zhou Y 2016 Mechanical stress in the superconducting film under external magnetic field *IEEE Trans. Appl. Supercond.* **26** 8402708
[42] Yong H D, Yang Y and Zhou Y H 2016 Dynamic fracture behavior of a crack in the bulk superconductor under electromagnetic force *Eng. Fract. Mech.* **158** 167–78
[43] Huang C G and Zhou Y H 2014 Magnetic and magnetostrictive properties of finite superconducting cylinders containing a cavity *J. Appl. Phys.* **115** 033904
[44] Xue F, Yong H and Zhou Y 2010 Effect of flux creep and viscous flux flow on flux-pinning-induced stress and magnetostriction in a long rectangular slab superconductor *J. Appl. Phys.* **108** 103910
[45] Yang Y and Wang X 2014 Magnetization and magnetoelastic behavior of a functionally graded rectangular superconductor slab *J. Appl. Phys.* **116** 023901
[46] Yang X and Tu S 2012 The effect of a constraining metal tube on flux pinning induced stress in a long cylindrical superconductor *J. Appl. Phys.* **112** 023909
[47] Zeng J, Wang X, Wu H, Xue F and Zhu J 2016 Kim model for flux-pinning-induced stress in a long cylindrical superconductor *AIP Adv.* **6** 075305
[48] Feng W, Han X and Ma P 2011 Flux-pinning-induced stress and magnetostriction in a functionally graded long rectangular superconductor slab *J. Appl. Phys.* **110** 063917
[49] Huang C G, Yong H D and Zhou Y H 2013 Magnetostrictive behaviors of type-II superconducting cylinders and rings with finite thickness *Supercond. Sci. Technol.* **26** 105007
[50] Yong H, Lu Y, Jing Z and Zhou Y 2016 Mechanical stress in the superconducting film under external magnetic field *IEEE Trans. Appl. Supercond.* **26** 8402708
[51] Yang X and Gan W 2013 Effect of thermal dilation stress and flux pinning induced stress on superconductor/tube system *J. Supercond. Nov. Magn.* **26** 3057–63
[52] Fujishiro H, Ainslie M, Takahashi K, Naito T, Yanagi Y, Itoh Y and Nakamura T 2017 Simulation studies of mechanical stresses in REBaCuO superconducting ring bulks with infinite and finite height reinforced by metal ring during field-cooled magnetization *Supercond. Sci. Technol.* **30** 085008
[53] Yang X, Li X, He Y, Wang X and Xu B 2017 Investigation on stresses of superconductors under pulsed magnetic fields based on multiphysics model *Physica* C **535** 1–8
[54] Fujishiro H, Hiyama T, Miura T, Naito T, Nariki S, Sakai N and Hirabayashi I 2009 Pulsed field magnetization for GdBaCuO bulk with stronger pinning characteristics *IEEE Trans. Appl. Supercond.* **19** 3545–8
[55] Fujishiro H, Tateiwa T and Hiyama T 2007 Enhancement of trapped field and total trapped flux on high temperature bulk superconductor by a new pulse-field magnetization method *Japan. J. Appl. Phys.* **46** 4108–12
[56] Rhyner J 1993 Magnetic properties and AC-losses of superconductors with power law current–voltage characteristics *Physica* C **212** 292–300
[57] Xia J and Zhou Y 2015 Numerical simulations of electromagnetic behavior and AC loss in rectangular bulk superconductor with an elliptical flaw under AC magnetic fields *Cryogenics* **69** 1–9
[58] Kim Y B, Hempstead C F and Strnad A R 1965 Flux-flow resistance in type-II superconductors *Phys. Rev.* **139** 1163–72
[59] Ainslie M D, Zhou D, Fujishiro H, Takahashi K, Shi Y H and Durrell J H 2016 Flux jump-assisted pulsed field magnetisation of high-J_c bulk high-temperature superconductors *Supercond. Sci. Technol.* **29** 124004
[60] COMSOL, Inc. www.comsol.com
[61] Zou S, Zermeno V M R, Baskys A, Patel A, Grilli F and Glowacki B A 2016 Simulation and experiments of stacks of high temperature superconducting coated conductors magnetized by pulsed field magnetization with multi-pulse technique *Supercond. Sci. Technol.* **30** 014010
[62] Konstantopoulou K, Shi Y H, Dennis A R, Durrell J H, Pastor J Y and Cardwell D A 2014 Mechanical characterization of GdBCO/Ag and YBCO single grains fabricated by top-seeded melt growth at 77 and 300 K *Supercond. Sci. Technol.* **27** 115011